AD_____

Award Number: DAMD17-98-1-8349

TITLE: ETACT-An Innovative Approach to Scintimammography

PRINCIPAL INVESTIGATOR: Frederic H. Fahey

CONTRACTING ORGANIZATION: Bowman Gray School of Medicine
Wake Forest University School of Medicine
Winston-Salem, North Carolina 27157

REPORT DATE: July 2001

TYPE OF REPORT: Annual

PREPARED FOR: U.S. Army Medical Research and Materiel Command
Fort Detrick, Maryland 21702-5012

DISTRIBUTION STATEMENT: Approved for Public Release;
Distribution Unlimited

REPORT DOCUMENTATION PAGE

Form Approved
OMB No. 074-0188

1. AGENCY USE ONLY (Leave blank)	2. REPORT DATE	3. REPORT TYPE AND DATES COVERED
	July 2001	Annual (1 Jul 00 - 30 Jun 01)

4. TITLE AND SUBTITLE
ETACT-An Innovative Approach to Scintimammography

5. FUNDING NUMBERS
DAMD17-98-1-8349

6. AUTHOR(S)
Frederic H. Fahey

7. PERFORMING ORGANIZATION NAME(S) AND ADDRESS(ES)

Bowman Gray School of Medicine
Wake Forest University School of Medicine
Winston-Salem, North Carolina 27157

E-Mail: ffahey@wfubmc.edu

8. PERFORMING ORGANIZATION REPORT NUMBER

9. SPONSORING / MONITORING AGENCY NAME(S) AND ADDRESS(ES)

U.S. Army Medical Research and Materiel Command
Fort Detrick, Maryland 21702-5012

10. SPONSORING / MONITORING AGENCY REPORT NUMBER

11. SUPPLEMENTARY NOTES

12a. DISTRIBUTION / AVAILABILITY STATEMENT
Approved for Public Release; Distribution Unlimited

12b. DISTRIBUTION CODE

13. ABSTRACT *(Maximum 200 Words)*

This project investigates the use of a novel approach to scintimammography (SMM) known as emission tuned aperture computed tomography (ETACT). In ETACT, a series of projections of the radionuclide distribution in the breast are acquired with fiducial markers. These data are reconstructed into tomographic slices. The hypothesis of this project is that ETACT will increase the diagnostic accuracy of SMM, and can be applied in a simple and practical manner. We have developed simulation models and have used these tools to investigate aperture size, angular disparity, number of projections, and the effect of attenuation and scatter. Apertures of 3-4 mm were determined to be optimal for ETACT. Smaller angular disparity of the projections led to slightly improved contrast but lower axial resolution. Seven projections is a good compromise between image quality and clinical practicality. Monte Carlo simulations have confirmed the findings of our simpler simulations that excluded the effects of scatter and attenuation. Biorthogonal merging of two ETACT image sets leads to improved lesion visualization. We are currently investigating the use of optical, fiducial markers, finalizing the phantom experiments and developing a clinical ETACT prototype.

14. SUBJECT TERMS
breast cancer, scintimammography, tomography

15. NUMBER OF PAGES
43

16. PRICE CODE

17. SECURITY CLASSIFICATION OF REPORT	18. SECURITY CLASSIFICATION OF THIS PAGE	19. SECURITY CLASSIFICATION OF ABSTRACT	20. LIMITATION OF ABSTRACT
Unclassified	Unclassified	Unclassified	Unlimited

Table Of Contents

Introduction

This project is investigating the use of a novel approach to scintimammography (SMM) known as emission tuned aperture computed tomography (ETACT). ETACT is based on the more general tuned aperture computed tomography (TACT) method used in radiography. TACT has been successfully applied in dentistry and its use in conventional mammography is currently being investigated. In ETACT, fiducial markers are placed around the object being imaged. A series of projection images are then acquired using a standard gamma camera with a pinhole (or other) collimator from any angle and at any distance, as long as all of the markers are within the field of view. The data are then reconstructed into a series of tomographic slices. This can be reconstructed easily on a PC. Thus ETACT requires no expensive, dedicated hardware. The beauty of this approach is that, if successful, this method could be applied in practically every hospital in the US, almost immediately. The main hypothesis of this project is that the application of ETACT will significantly increase the diagnostic and prognostic accuracy of SMM, particularly for small, nonpalpable lesions, and that this innovative method can be applied in the clinic in a simple, flexible and practical manner. The specific aims of this research are as follows:

1. to develop and utilize a computer simulation model of ETACT to determine the optimal parameters for its application and to compare it to conventional SMM,
2. to utilize phantom data to further compare ETACT to conventional SMM, both planar and SPECT, and
3. to design a clinical ETACT prototype system that will then be used in a subsequent preliminary clinical investigation.

In this report, we will present our progress in further development of computer simulation and Monte Carlo models of ETACT, the results from these models, the development of an approach to merge orthogonal ETACT data sets, and the investigation of the use of optical rather than radioactive fiducial markers. Since we have been granted a one-year extension for this project, we will discuss the changes in our approach that has been dictated by these preliminary results and present an outline for the remainder of this project.

Body of the Report

I. ETACT

In ETACT, one or more fiducial markers are placed about the patient's breast. A series of projection images are acquired with a pinhole-collimated, gamma camera. We use pinhole collimation for three reasons. First, pinhole collimators are routinely available for most portable, gamma cameras, making this method a straightforward approach that can be applied in practically any hospital. Secondly, we plan to take advantage of the high resolution associated with pinhole collimation. For a typical pinhole collimator of length 30 cm and pinhole diameter of 4 mm as well as an intrinsic spatial resolution of the detector of 3.5 mm, the system spatial resolution is approximately 5 mm compared to that of planar and SPECT imaging with a high resolution collimator of approximately 7 mm and 10 mm, respectively. Special inserts could also be made that would reduce the pinhole diameter improving the resolution. Thirdly, the collimator sensitivity is inversely proportional to the square of the aperture-to-object distance whereas the sensitivity of a parallel hole collimator does not vary with collimator-to-object distance, thus reducing the contribution to the image of activity in other organs such as the heart of the liver.

Consider the technique known as "tomosynthesis" (Grant 1972). In this case, the detector (the gamma camera crystal) is always oriented parallel to the tomographic plane of interest. Several projections are acquired such that all of the aperture (pinhole) locations are known, coplanar and parallel to the tomographic plane of interest. A series of tomographic planes can be reconstructed by appropriately shifting the projection data and adding them together. All reconstructed planes are parallel to the detector plane. Tomosynthesis has been shown to be a very simple and effective manner of generating tomographic data. However, it places many constraints on the acquired projection data, and the aperture locations for all of the projections must be known.

ETACT alleviates these geometric constraints by using the projected locations of a series of fiducial markers to obtain knowledge concerning each projection (Fahey 2001, Webber 1997). Consider the case where the detector is still coplanar and parallel to the tomographic plane of interest, but the actual location is not known. A fiducial marker whose location relative to the object is fixed is also imaged within each projection. Consider a reference plane whose location is the same as the aperture to detector distance, but whose location is opposite the detector (see Figure 3,

Fahey 2001. *NB*: This reference in included in the Appendix). If we overlay all of the projections and add them, we are reconstructing the reference plane. If we determine the centroid of the projected locations of the marker, shift all of the data such that projected location of the marker coincides with the centroid and add the data together, we would reconstruct the plane that contains the fiducial marker and is parallel to the detector plane. If the projections are shifted by half that amount and added, then the plane that is half way between the marker and the reference plane is reconstructed. In this manner, any arbitrary plane can be reconstructed.

In the present implementation of ETACT, 5 markers are used, four of which are coplanar and one of which is not. The four coplanar markers are used to transform all of the acquired projections such that they appear to all have been acquired with the aperture in a common plane. The fifth marker is then used as described above to shift and add the projections to reconstruct the series of tomographic slices. It also has been demonstrated that this approach with the five fiducial markers can be used to reconstruct the data even if the detector in each projection is not in the same plane.

In summary, if we acquire a series of projection images using a set of 5 fiducial markers (4 coplanar and one out of plane), we can reconstruct the data into a series of tomographic slices, even if the location of neither the detector nor the aperture is known. It is also not necessary to have the detector in the same plane or at the same distance in each projection. Therefore, ETACT is a simple and flexible method of acquiring and processing tomographic data.

II. Further Development of ETACT Simulation Models

In the past, we reported the development of a computerized, simulation model of the acquisition of ETACT data. The model currently allows you to define an arbitrary 3D object with a set of markers. The activity associated with each component can be defined. Once the detector configuration and the object are defined, the detector can be moved interactively about object and simulated projections obtained. These data can be subsequently reconstructed with the standard, ETACT software. The projections are then blurred to the resolution and Poisson noise added that were consistent with the aperture size chosen. We have used this simulation model to evaluate the effect of the aperture size, angular disparity and the number of projections on contrast and signal-to-noise.

In order to evaluate the effect of photon attenuation and scatter on the above simulations, we utilized the MCNP Monte Carlo simulation code to model ETACT. MCNP has been shown to provide similar results to the EGS4 code. In these simulations, the breast was modeled as a 15 cm hemisphere and the tumor as a 7.5 mm sphere. The pinhole diameter was 6 mm. The acquisition geometry consisted of 25 cm pinhole-to-detector distance and a 15 cm pinhole-to-tumor distance, the same as in the ray-tracing simulations. In these simulations, three cases were considered: uncollided gamma rays (attenuation but no scatter), total attenuated (attenuation and scatter) and unattenuated. These were compared to evaluate the effects of photon attenuation and scatter.

III. Evaluation of Aperture Size, Angular Disparity and Number of Projections Through Simulation

We modeled the breast as a hemisphere with 15 cm diameter. The tumor was modeled as a sphere in the center of the breast. We considered 3 tumor sizes (5, 7.5 and 10 mm) and 2 target-to-nontarget (T/NT) ratios (5:1 and 10:1). Five markers (4 coplanar and one out-of-plane) were placed lateral to the breast. The detector was modeled as a gamma camera with a 50x50 cm filed-of-view. The aperture-to-detector distance was 25 cm. The aperture sizes (diameters) used were 1, 2, 3, 4, 5 and 6 mm. The aperture-to-object distance of approximately 15 cm was chosen such that the object, including the markers, took up the majority of the field of view. Using our projection simulator, we constructed 7 noiseless projections for each aperture size. We investigated 3 angular disparities between the projections: +/- 10, 15 and 20 degrees. Based on the calculated system spatial resolution of each pinhole, the projection data were blurred with a gaussian kernel. Based on the sensitivity of each pinhole size, Poisson noise was added to each pixel. These data were then reconstructed using the standard TACT reconstruction software.

To evaluate these data, the slice through the middle of the tumor was visually selected and a region of interest (ROI) was drawn about the tumor and the maximum pixel value (Max) in the ROI was determined. A similar sized and shaped ROI was placed lateral to the tumor to evaluate the background activity. The mean pixel value (BKG) and the standard deviation (SD_{BKG}) in the background ROI were determined. The contrast (C) was calculated using the formula

$$C = \frac{Max - BKG}{BKG}$$

A detectability index referred to as the contrast-to-noise ratio (CNR) was calculated by

$$CNR = \frac{C}{(SD_{BKG}/BKG)}$$

The results of this investigation are summarized in the Tables 2 and 3 of (Fahey 2001). As the aperture size is reduced, the contrast improves. This is expected due to the improved resolution and the subsequent reduction in the partial volume effect. However, the sensitivity decreases with reduced aperture size leading to fewer photons being acquired and thus a noisier image. Therefore, a 3 mm aperture is optimum with respect to the CNR although not substantially better than the 4 mm aperture.

The results of the angular disparity study are shown in the table below.

Contrast

Disparity Angle	10/10	10/5	7.5/10	7.5/5	5/10	5/5
10 degrees	0.36	0.28	0.29	0.12	0.08	0.07
15 degrees	0.37	0.25	0.27	0.09	0.06	0.06
20 degrees	0.25	0.24	0.22	0.06	0.07	0.07

In the above table, the designation A/B indicates a tumor diameter in mm of A and a tumor-to-nontumor ratio of B. For example, 10/5 indicates a 10 mm tumor with a 5:1 tumor-to-nontumor ratio. As can be seen, the contrast increases slightly with decreasing angular disparity. However, smaller angular disparity yields poorer axial spatial resolution. For example, no angular disparity yields a simple planar image with no axial resolution. From these results, a 15 degree angular disparity is a reasonable choice. Increasing the number of projections without increasing the total number of counts was shown to lead to an increase in contrast. If one knew the best, single projection to acquire, it may have higher contrast than ETACT, but one does not know the best projection *a priori*. Thus, ETACT typically provides higher contrast than planar imaging. With more projections, there will be more set-up time extending the length of the study. Therefore, seven projections is a reasonable number for the clinical implementation of ETACT.

IV. Monte Carlo Simulation Results

The results of the Monte Carlo simulation are shown in Figure 1 (see Appendix). This figure shows profiles of the counts through the tumor and breast for the three cases: uncollided, attenuated and no attenuation. The "no attenuation" case corresponds to case used in the ray-tracing simulations. As shown in the figure, the three profiles are very similar except for the scale resulting from photon attenuation. The contrast for these cases is very similar. This study validates the conclusions drawn from the ray-tracing simulations.

V. Biorthogonal Imaging

All methods based on tomosynthesis yield poor resolution and streak artifacts in the direction orthogonal to the tomographic planes. We investigated whether combining the data from two orthogonal TACT data sets would minimize these artifacts (Webber 2001). This study was performed on transmission, mammographic data. A frozen autopsy breast sample was placed in a 35 mm cardboard box. Small lead markers ("Beekly spots") were placed on the corners of the box. The box was radiographed from 5 angles at angular disparities of -15, -7.5,0, 7.5 and 15 degrees. The box was then rotated 90 degrees and an analogous set of projections was acquired. The two data sets were reconstructed independently using the TACT algorithm and corrected for differential magnification between slices. The two 3D data sets were then combined via simple averaging of the pixel values. Projections through this merged data set were rendered either by linear averaging or by plotting the maximum value along each ray.

The results are illustrated in Figures 4 and 5 of (Webber 2001. *N.B.* This article is included in the Appendix). These figures show the linear and the maximum rendering, respectively. As can be seen, the individual image sets are well resolved in the direction normal to the reconstruction planes but resolution is substantially degraded in the orthogonal direction. However, the merged data set is well resolved at all angles. Although this experiment was performed with transmission data, the conclusions are applicable to ETACT as well. We plan to validate this in the next year.

VI. Use of Optical Fiducial Markers

The results from our simulation experiments indicate that we have to image at a substantial distance in order to include all of the fiducial markers in each projection Imaging at such a distance leads to a substantial loss in the effectiveness of the pinhole collimator. The sensitivity of the pinhole collimator falls off as the inverse square of the object-to-aperture distance. Therefore, if we could reduce the aperture-to-object distance by a factor of 2, we would see a 4 fold increase in the number of counts and the noise level would decrease by half. Alternatively, we could either reduce the imaging time or improve the spatial resolution by using a smaller aperture size. At the same time, the spatial resolution of the systems dramatically improves with a shorter imaging distance. In addition, radioactive markers can be troublesome to make. For these reasons, we are investigating the use of optical fiducial markers. This is accomplished by mounting a digital camera on the gamma camera and acquiring both nuclear and optical images at each projection angle. The fiducial markers on the optical images are then used to reconstruct the radiologic image. After a thorough mathematical evaluation, we have determined that the optical image can be used *without* cross-calibration to the radiologic image, as long as the digital camera and the radiologic camera (e.g. gamma camera) are oriented such that they are both the same distance from the image plane and they are not rotated about the object in that plane. We are currently running phantom studies to validate this in both radiographic TACT and ETACT.

VII. Summary of Preliminary Evaluation and Future Directions

It should be noted that we have been granted a one-year extension to complete this project. Thus far we have shown that ETACT can be performed in a practical manner and that it provides enhanced contrast relative to planar SMM. We have determined that acquiring about 7 projections with 15 degree disparity using a 3-4 mm pinhole is reasonable. In the next year, we will continue to investigate the merging of orthogonal ETACT data sets to improve the detectability of small lesions. We will also investigate the use of optical fiducial markers. Once we finalize our ETACT methodology, we will complete our phantom studies comparing ETACT to both planar and SPECT SMM.

VII. Review of Statement of Work

In this section, we will review the original statement of work and review the status of each component. We have been granted a one-year extension for this project, so some tasks will be completed in Months 37-48. The review on current status for each step will be in square brackets [] and italicized so that it will be easily distinguishable from the original task.

Task 1: To develop and utilize a computer simulation model (Months 1-15) [*This has been completed.*]

- Develop female, thoracic computer phantom including breasts, tumor, lymph nodes, heart, liver and lungs [*This has been completed.*]
- Model radiologic properties of phantom including emission, detection, attenuation, scatter and Poisson noise [*This has been completed*]
- Model ETACT with number of fiducial markers, placement of markers, number and orientation of ETACT views [*This has been completed*]
- Model conventional SMM including both planar and SPECT [*This has been completed*]
- Run simulations varying lesion size, location and T/NT ratio [*This has been completed.*]
- Determine SNR and perform ROC analysis to compare different ETACT configurations to each other and to conventional SMM [*This has been completed.*]

Task 2: To acquire and utilize phantom data to further compare ETACT to conventional SMM (*New estimate Months 6-48*)

- Develop phantom protocol including lesion placement, size and T/NT ratio and activity in other organs (heart, liver and chest) [*This has been completed*]
- Acquire ETACT data with portable gamma camera and pinhole collimator varying number and location of fiducial markers, number and location of views and reconstruction method [*This has been completed*]
- Acquire conventional SMM including planar and SPECT [*We have acquired the planar data. We will acquire the SPECT data in Months 37-40*]
- Perform ROI analysis to determine the SNR in the phantom data [*This will be done in Months 40-44*]
- Perform ROC analysis to compare different implementations of ETACT to each other and to conventional SMM [*This will be done in Months 42-46*]

Task 3: To design a clinical ETACT scintimammographic system prototype (*New estimate Months 36-48*)

- Based on results of Tasks 1 and 2, design the optimal, acquisition parameters for ETACT SMM [*This will be done in Months 40-44*]
- Design a system for reliable and practical method of marker placement [*This will be done in Months 37-40*]
- Review design with both technical and physician staff in both nuclear medicine and mammography [*This will be done in Months 45-48*]
- Modify and finalize design based on clinical feedback. [*This will be done in Months 45-48*]

Key Research Accomplishments

Task 1: To develop and utilize a computer simulation model

- We have developed a 3D tool for simulating the ETACT acquisition process including emission, pinhole collimation, detection and Poisson noise.
- We have developed a simple breast tumor model for the evaluation of scintimammography.
- We have migrated this application from SGI to NT to make it more accessible.
- We have performed an evaluation of the aperture size, angular disparity and number of projections using the simulation application described above.
- We have developed a Monte Carlo model of ETACT and used it to evaluate the effect of photon attenuation and scatter on ETACT.

Task 2: To acquire and utilize phantom data to further compare ETACT to conventional SMM

- We have acquired the Data Spectrum breast phantom and have developed a protocol for imaging this phantom with fiducial markers using a portable gamma camera with a pinhole collimator.
- We have acquired a preliminary comparison between ETACT and planar SMM using phantom data.
- We have validated our simulation results and shown ETACT to be a clinically practical approach.

Task 3: To design a clinical ETACT scintimammographic system prototype

- We have developed a method of merging two orthogonal ETACT data sets to further improve image quality and tumor detectability.
- We have determined mathematically that optical fiducial markers can be applied to ETACT in a practical manner.

Reportable Outcomes

Fahey FH, Webber RL, Harkness BA. ETACT: a novel approach to scintimammography. J Nucl Med 1998; 39:24P (abstract, presented at the Society of Nuclear Medicine Annual Meeting, Toronto, June 1998)

Fahey FH, Webber RL, Bayram E, Harkness BA, Mu Z, Hemler P. Preliminary evaluation of ETACT scintimammography. Med Phys 1999; 26:1072 (abstract, presented at the American Association of Physicists in Medicine Annual Meeting, Nashville, July 1999)

Hemler PF, Webber RL, Fahey FH. Modeling and error identification of three dimensional tomosynthesis reconstructions. SPIE Proceedings. 2000;3979:1280-1287 (presented at the SPIE Symposium on Medical Imaging, February 2000)

Fahey FH, Grow KL, Webber RL, Bayram E, Harkness BA, Hemler PF. ETACT: A Novel Approach to Scintimammography. ERA of Hope Proceedings, Vol 1. 2000. (abstract, presented at the Era of Hope Meeting, Atlanta, June 2000)

Grow KL. Evaluation of emission tuned aperture computed tomography. Masters Thesis. Wake Forest University, 2000.

Fahey FH, Grow KL, Webber RL, Harkness BA, Bayram E, Hemler PF. Emission tuned-aperture computed tomography: a novel approach to scintimammography. J Nucl Med 2001;42:1121-1127.

Webber RL, Fahey FH. Biorthogonal merging of mammographic slices using tuned-aperture computed tomography. (Submitted to J Elect Imag).

Fahey FH, Grow KL, Meltsner MA, Webber RL. Angular disparity in ETACT scintimammography (abstract, accepted for presentation at Radiologic Society of North America, Chicago, November 2001).

Conclusions

We have implemented the ETACT reconstruction algorithm that we described in our application. We have further developed a computerized simulation model for the acquisition process associated with ETACT including emission, collimation, detection and Poisson noise. We have also developed a simple model for the breast with a small tumor which also includes the fiducial markers necessary for doing ETACT. We used these simulation tools to perform an evaluation of the aperture size, angular disparity and number of projections. Based on this evaluation, it was determined that a 3-4 mm diameter aperture was optimal for ETACT. We also developed a Monte Carlo model of ETACT that included attenuation and scatter to demonstrate the validity of our ray-tracing simulation results. Using this phantom, we performed a preliminary evaluation to test the validity of our simulations and the feasibility of this approach. These evaluations indicated that we need to greatly reduce the aperture-to-object distance if we are to improve the performance of ETACT. In order to accomplish this, we are investigating the use of optical fiducial markers with a digital camera. We also demonstrated that merging 2 orthogonal ETACT data sets greatly improve image quality and tumor detectability.

We have been granted a one-year extension for this project. In the next year, we will finalize the investigation of the use of optical fiducial markers. Based these and our previous results, we will develop a methodology for the clinical implementation of ETACT. Using this methodology, we will finalize our phantom studies and complete or comparison of ETACT to both planar and SPECT SMM. We will then consult with our clinical colleagues and finalize of clinical ETACT prototype.

References

Fahey FH, Grow KL, Webber RL, Harkness BA, Bayram E, Hemler PF. Emission tuned-aperture computed tomography: a novel approach to scintimammography. J Nucl Med 2001;42:1121-1127.

Grant DG, Tomosynthesis: A three-dimensional radiographic imaging technique. IEEE Trans Biomed Engin 1972; BME-19:20-28.

Webber RL, Horton RA, Tyndall DA, Ludlow JB. Tuned-aperture computed tomography (TACT™). Theory and application for three-dimensional dento-alveolar imaging. Dentomaxill Radiol 1997; 26:53-62.

Webber RL, Fahey FH. Biorthogonal merging of mammographic slices using tuned-aperture computed tomography. (Submitted to J Elect Imag).

Appendix

This appendix includes the Figure 1 from the *Body of the Report* and

Fahey FH, Grow KL, Webber RL, Harkness BA, Bayram E, Hemler PF. Emission tuned-aperture computed tomography: a novel approach to scintimammography. J Nucl Med 2001;42:1121-1127.

Webber RL, Fahey FH. Biorthogonal merging of mammographic slices using tuned-aperture computed tomography. (Submitted to J Elect Imag).

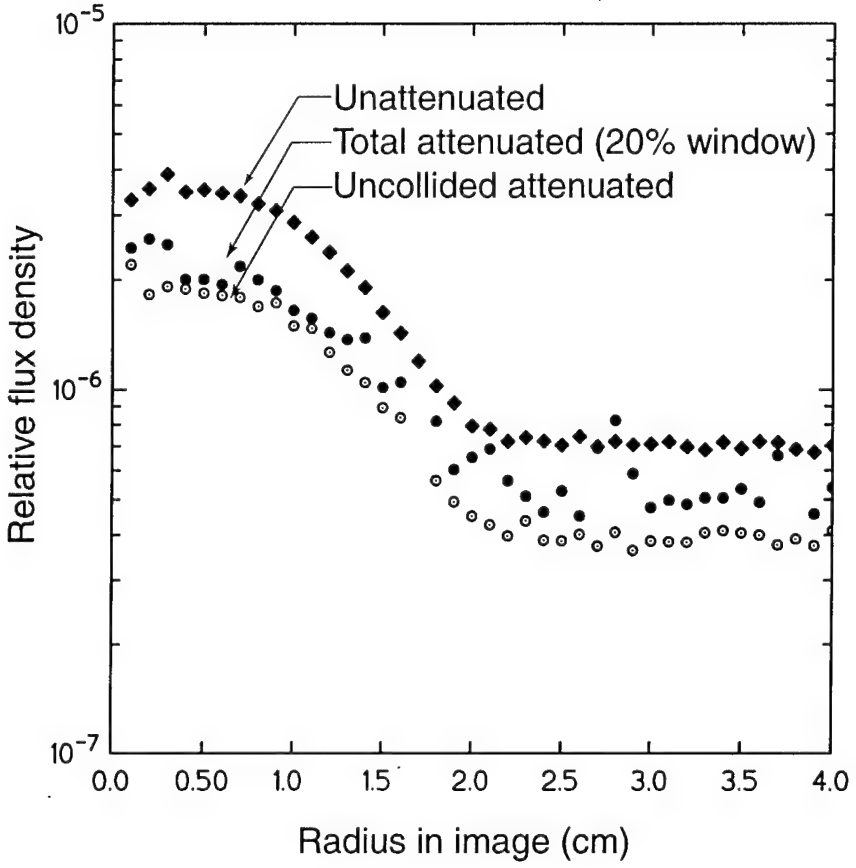
Unattenuated
Total attenuated (20% window)
Uncollided attenuated
Relative flux density
10^{-5}
10^{-6}
10^{-7}
0.0
0.50
1.0
1.5
2.0
2.5
3.0
3.5
4.0
Radius in image (cm)

Figure 1

Emission Tuned-Aperture Computed Tomography: A Novel Approach to Scintimammography

Frederic H. Fahey, Kerry L. Grow, Richard L. Webber, Beth A. Harkness, Ersin Bayram, and Paul F. Hemler

Division of Radiologic Sciences, Wake Forest University School of Medicine, and Department of Physics, Wake Forest University, Winston-Salem, North Carolina

Emission tuned-aperture computed tomography (ETACT) is a new approach to acquiring and processing scintimammography data. A gamma camera with a pinhole collimator is used to acquire projections of the radionuclide distribution within the breast. Fiducial markers are used to reconstruct these projections into tomographic slices. Simulation and phantom experiments were performed to evaluate the potential of the ETACT method. **Methods:** In the simulation study, a hemispheric object of 15 cm in diameter was constructed to model a breast. A ray-tracing technique was used to generate ideal projections. These were blurred and noise was added to create images that resemble scintigraphic images. Tumor size, pinhole size, and target-to-nontarget radioactivity ratios (TNTs) were varied. The simulated projections were reconstructed into slices, and contrast and contrast-to-noise ratios were calculated to evaluate the effect of pinhole size. These results were compared with a simulated planar acquisition of the same object. A preliminary phantom evaluation was performed using an 8-mm "tumor" with a 10:1 TNT to validate the simulation results. **Results:** A 3-mm pinhole was shown by the simulation study to be the optimal size. The ETACT images consistently yielded higher contrast than simulated planar images. The phantom study validated the simulation results and showed the feasibility of ETACT in a simulated clinical environment. **Conclusion:** ETACT is shown to be useful for imaging tumors <1 cm in diameter. Because ETACT requires only a gamma camera with a pinhole collimator, it has the potential to be applied in any hospital in a simple, flexible, and practical manner.

Key Words: tomography; pinhole collimation; reconstruction

J Nucl Med 2001; 42:1121–1127

Breast cancer is the most common malignancy among women in the United States (*1*). Every year, more than 185,000 lives are impacted as a result of breast cancer and 44,000 die of the disease (*2*). Patients with breast cancer diagnosed at a localized stage experience a survival rate of 90%, whereas the rate is <20% if the cancer has spread to 1 or more distant sites (*3*). Early detection, therefore, plays an essential role in the fight against breast cancer. Although mammography is currently the best imaging approach for breast cancer screening, several factors may limit its accuracy. Dense breasts, breast implants, or scars may either resemble a tumor or hide true small tumors on the mammogram. As a result, false-positive as well as false-negative incidents are increased. Mammography has a relatively high sensitivity (88%), although dense or large breasts may reduce this. However, it has a low specificity (67%) (*4*).

Scintimammography using ^{99m}Tc-labeled sestamibi has been shown to have high sensitivity and specificity (93.7% and 87.8%, respectively) for tumors >1.5 cm (*5*). However, in its current implementation, the limited spatial resolution of the gamma camera limits the sensitivity and specificity for tumors <1 cm (*6*). We are developing a new approach to detect early stages of breast cancer with scintimammography called emission tuned-aperture computed tomography (ETACT). ETACT uses pinhole collimation and limited angle tomography to potentially improve the contrast of small tumors. In this article, we describe the ETACT method and present some preliminary simulation and phantom investigations of this approach.

ETACT is based on the tuned-aperture computed tomography (TACT) method developed by Webber et al. (*7*). Consider the tomographic method known as tomosynthesis (*8*). In tomosynthesis, several planes through an object are reconstructed from a small number of 2-dimensional (2D) projections. This technique is illustrated in Figure 1. A series of coplanar x-ray sources form a circular pattern. A disk and a square are located between the source and detector planes. Each source projects the 2 objects onto the detector plane, resulting in a series of projections. By shifting by the appropriate amount and then adding these projections, any plane through the object can be reconstructed. For instance, if all projections are shifted so that the centers of the disk in all images are aligned and the projections are then added together, the result is the slice that contains the disk being reconstructed. Note that the square object is out of focus in this plane. However, by shifting such that the squares align and then adding, the plane through the square

Received Nov. 2, 2000; revision accepted Mar. 8, 2001.

For correspondence or reprints contact: Frederic H. Fahey, DSc, PET Center, Wake Forest University School of Medicine, Medical Center Blvd., Winston-Salem, NC 27157-1061.

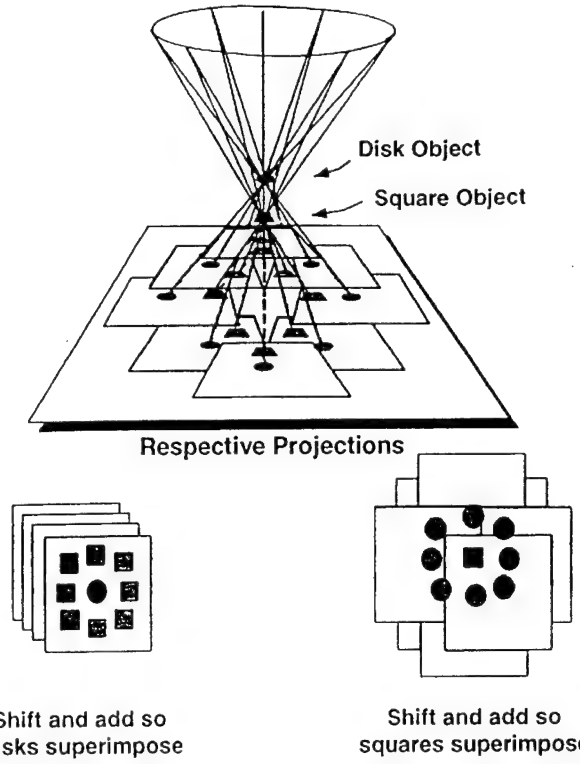

FIGURE 1. Tomosynthesis is imaging technique that shifts and adds series of 2D projections to construct 3-dimensional image. Point sources of each projection are coplanar, leading to linear shifting and adding of projections. Through shifting and adding process, any arbitrary slice through object can be reconstructed. (Reprinted with permission of (*7*).)

can also be reconstructed. In this fashion, any slice through the object can be created, and a 3-dimensional (3D) representation of the object is constructed. In tomosynthesis, the amount to shift the projections before addition is determined from the known location of the x-ray sources.

In TACT, the imaging geometry is more flexible and the source is not restricted to 1 plane. This allows more freedom to "tune" the projections to each situation, thus optimizing the reconstruction. As a result of this loosened geometry, fiducial markers are needed to compensate for the extra degrees of freedom. First, consider the sources to be located in a plane parallel to the detector plane, but with unknown position within that plane, as shown in Figure 2. A single fiducial marker is used. If all projections are added without shifting, we are reconstructing the detector plane. The centroid of the fiducial marker locations in all projections is then calculated. The projections are shifted such that the locations of the fiducial marker in the different projections align with the centroid and are then added together. The result is the reconstruction of the slice containing the fiducial marker as shown in Figure 2. To reconstruct a slice one third of the way between the marker and the detector plane, the projections are shifted two thirds the distance between their initial location and the centroid and added together. In this fashion any arbitrary slice can be reconstructed and a 3D representation of the object is constructed (*7*).

Now consider a situation in which the source locations are not coplanar and their locations are unknown. In this case, at least 5 fiducial markers (e.g., 4 coplanar and 1 out of plane) are needed. The 4 coplanar markers are used to apply a projective transformation between the projections and a reference image. This provides a correction for skewing and a first-order correction for magnification. The magnification correction applies only to the plane containing the 4 fiducial markers and does not correct for the differential magnification between planes. Once this transformation has been applied to the projections, they can be treated as if they were acquired with coplanar sources and the fifth, out-of-plane fiducial marker is used to reconstruct the data as described previously (i.e., shifting and adding). TACT has been used successfully in a variety of radiographic applications including dental radiography and mammography (*7,9*).

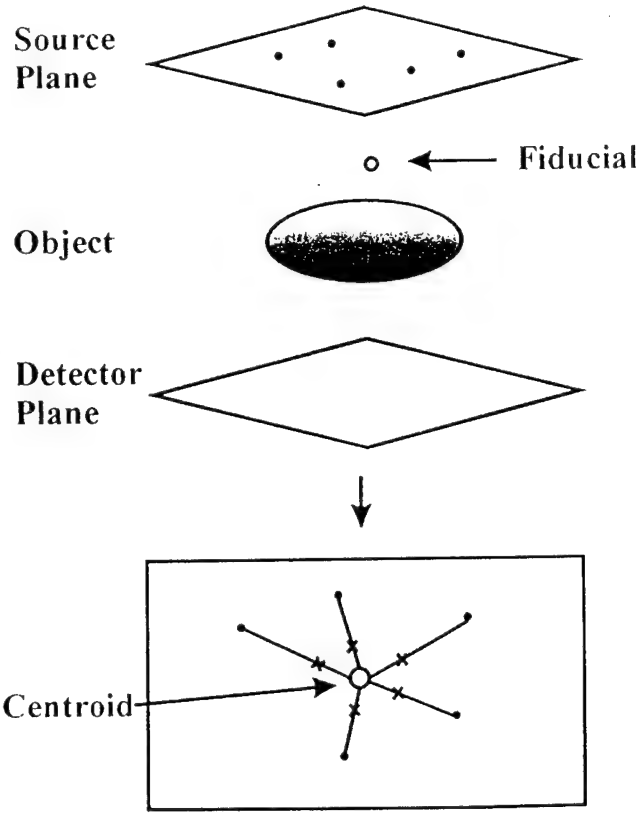

FIGURE 2. Demonstration of concepts of TACT. Five x-ray source locations are coplanar but arbitrary and unknown. One fiducial marker is used. Five projections of object are obtained. If projections are added without shifting, object at detector plane is reconstructed. Centroid of 5 marker locations is determined. If all projections are shifted such that marker locations align with centroid and projections are then added, plane containing fiducial marker is reconstructed. To reconstruct plane one third of way from marker to detector plane, projections are shifted two thirds of distance from their initial location toward centroid and then added. In this manner, any arbitrary plane can be reconstructed and 3D representation of object is obtained.

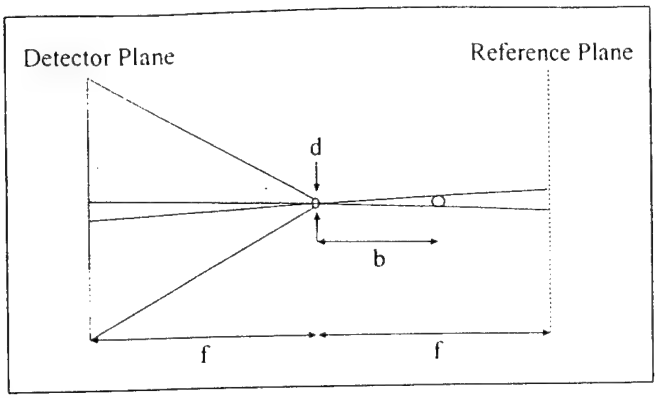

FIGURE 3. Similarity between TACT and ETACT geometry, where d is pinhole diameter, b is pinhole-to-object distance, and f is distance from pinhole to both detector and reference planes. In ETACT, reference plane is parallel to detector plane and same distance from pinhole, but on opposite side of pinhole. In ETACT, pinhole is analogous to source in TACT.

ETACT is emission TACT, which combines the concept of TACT with nuclear medicine imaging. A radiopharmaceutical is injected into the patient and imaged with a gamma camera using a pinhole collimator. In this geometry, the x-ray source in TACT is replaced with the pinhole collimator. The detector plane is the surface of the NaI detector. A reference plane is defined that is parallel to the detector plane and equidistant to the pinhole but on the opposite side, as shown in Figure 3. The pinhole location is not restricted to 1 plane. This allows the freedom to choose projection angles, which will be optimized for each specific imaging situation. The 5 fiducial markers are radioactive in ETACT. After the projective transformation of the projections (using the 4 coplanar markers), adding the projections without shifting reconstructs the reference plane. Shifting all projections so that the fifth fiducial marker locations in all images align with their centroid reconstructs the plane parallel to the reference plane and containing the fifth marker. Shifting the projections a set fraction of that amount reconstructs the plane that is that fraction of the distance between the fifth fiducial marker and the reference plane. Therefore, ETACT can reconstruct any number of slices and thereby generate a 3D representation of the object.

Potential benefits of ETACT arise from both the use of pinhole collimation and the flexibility of the ETACT acquisition. In the first case, the pinhole collimator provides superior spatial resolution to that of a parallel-hole collimator. For a pinhole-to-detector distance of 25 cm, a pinhole diameter of 4 mm, and an intrinsic spatial resolution of 3.5 mm, the pinhole system spatial resolution is approximately 6.0 mm compared with that of planar and SPECT imaging with a high-resolution collimator, which would be approximately 7.5 and 10 mm, respectively. This increased spatial resolution will lead to enhanced contrast of small tumors attributed to a reduction in the partial-volume effect. Second, the sensitivity of the pinhole collimator is inversely proportional to the square of the pinhole-to-object distance, whereas the sensitivity of a parallel-hole collimator does not vary with distance. Therefore, the pinhole collimator will be less sensitive to activity in objects behind the breast such as the myocardium or the liver. For example, if we assume that radioactivity in the tumor and myocardium is located 7 and 14 cm from the pinhole, respectively, then the system will be 4 times more sensitive to activity in the tumor than it is to the myocardium.

The advantage of ETACT over other tomographic methods is that the 3D resolution as well as the signal to noise can be "tuned" to specific diagnostic tasks through purposeful manipulation of the data-sampling strategy. This is analogous to altering one's vantage point to optimize the viewing of a scene or manipulating the optical aperture of a camera to adjust the depth of focus to best fit the imaging task at hand. Therefore, the projections obtained during an ETACT acquisition can be chosen to avoid signals from other organs such as the heart or liver or to enhance the tomographic capability for challenging imaging tasks such as the detection of small tumors near the chest wall.

On the basis of both of these factors, ETACT has the potential to enhance the detection of small tumors in the breast. Pinhole collimation enhances system spatial resolution and degrades the contribution of signal from other organs, and TACT reconstruction further enhances the contrast of these small structures. The result should be an overall increase in the signal-to-noise ratio (SNR) and, thereby, detectability for small tumors. Clinically, this should result in improvements in sensitivity and specificity for the detection of breast tumors <1 cm in diameter.

MATERIALS AND METHODS

Simulation Experiments

Simulation studies were used to determine the optimal pinhole size for ETACT. An object was designed whose shape resembled that of a hemispheric breast, 15 cm in diameter. A spheric tumor was placed in the center of the breast. The tumor was assigned a diameter of 5, 7.5, or 10 mm. Five fiducial markers were placed to the lateral side of the breast. Four of the markers were coplanar (parallel to a sagittal plane through the breast) and formed a square, 5×5 cm, whereas the fifth fiducial marker was out of the plane by 1 cm. The target-to-nontarget radioactivity ratio (TNT) was also defined. In various simulations the TNT was 5:1 (i.e., the tumor was 5 times as "hot" as the rest of the breast), 7.5:1, 10:1, 12.5:1, or 15:1. The 3D object was represented as a series of 40 equally spaced slices. Projections of this object were generated using a ray-tracing technique (*10*). The detector was defined as a 500×500 mm square to ensure that all projections would be within the field of view. The pinhole-to-detector and pinhole-to-object (tumor) distances were 25 and 15 cm, respectively. A symmetric set of angles was used to take 7 projections of the object. The first image was a straight lateral view of the breast. From the straight lateral, let the angle θ describe the amount of caudal tilt and the angle ϕ describe the amount of rotation about the long axis of the body. The other 6 projections were acquired in a hexagonal pattern with each view 15° from the straight lateral as described in Table 1. Note that $\theta = 10°$ and $\phi = 10°$ lead to an angle from the straight lateral of about 15°. These 7 projections

TABLE 1
Angular Orientation of Each Simulated Projection

Projection	Angle (°)	
	θ	ϕ
1	0	0
2	15	0
3	−15	0
4	10	10
5	−10	10
6	10	−10
7	−10	−10

From straight lateral, let angle θ describe amount of caudal tilt and angle ϕ describe amount of rotation about long axis of body. Note that θ = 10° and ϕ = 10° lead to angle from straight lateral of about 15°.

were considered "ideal," meaning no blurring or noise was added. These projections were then blurred and noise was added, depending on the pinhole size, which was varied: 1, 2, 3, 4, 5, and 6 mm in diameter. The blurring was accomplished by convolving the projections with a gaussian kernel having SD σ with:

$$\sigma = R_{sys}/2.35,$$

$$\text{with } R_{sys} = (R_{ph}^2 + (R_I/M)^2)^{1/2},$$

$$R_{ph} = \frac{d}{f}(f + b),$$

$$\text{and } M = \frac{f}{b},$$

where d is the pinhole diameter, f is the pinhole-to-detector distance, b is the pinhole-to-object distance, M is the magnification factor, R_I is the intrinsic resolution, R_{sys} is the system resolution, and R_{ph} is the pinhole resolution (*11*).

Noise was then added to each projection. First, the projection data were scaled such that the pixel values were similar to that acquired with a gamma camera using a pinhole collimator. The sensitivity was calculated on the basis of the pinhole size, using (*11*):

$$G = \frac{1}{16}(d/f)^2(b + f).$$

The scaled projection was multiplied by the sensitivity on a pixel-by-pixel basis. Each pixel value was sampled from a Poisson distribution with a mean N, where N is the noiseless pixel value. Projection sets were generated for various tumor sizes, TNTs, and pinhole sizes. All sets were simulated twice, once using blurred data and once using data that were both blurred and noisy. A total of 36 ideal projection sets was simulated.

For each projection set, the TACT software developed by R.A. Horton and R.L. Webber (Verity Software Systems, Winston-Salem, NC) was used to reconstruct the data. The straight lateral view was used as the reference. The 4 coplanar fiducial markers were identified on each projection, and a projective transformation of each of the projection images was performed. The fifth marker was identified in each projection and used to determine the amount of shifting necessary to reconstruct different slices through the object. Figure 4 displays 4 of 40 reconstructed slices of the blurred and noisy case for the 10-mm tumor and 10:1 TNT and a 3-mm pinhole. Because the lateral view was used in each case as the reference image, all reconstructed image sets were oriented in the same way. For each case, the slice with the tumor was selected. Contrast measurements of tumor counts versus background counts in the blurred image were calculated and recorded. A 16 × 16 pixel region of interest (ROI) was used to determine the counts over the tumor. A similarly sized ROI was placed in the background of the breast, just outside of the tumor boundary. Two measurements were made in the background and then averaged. One measurement was made directly on the tumor and the value (TUM) was recorded. The contrast was then estimated using the following formula:

$$C = \frac{(TUM - BKG)}{BKG},$$

where BKG is the mean value of the pixel counts in a background ROI. The fractional SD (FSD = SD/BKG) of the pixel values in the background of the blurred and noisy image was also calculated. Two FSD measurements were taken from the background of the breast and then averaged together. The contrast, C, was divided by the averaged FSD to estimate the contrast-to-noise ratio (CNR):

$$CNR = \frac{C}{FSD}.$$

The CNR is analogous to the SNR. Calculation of the SNR would require the fractional SD of the ROI counts rather than the pixel counts. However, if the pixel counts in the region are reasonably uniform, the 2 SDs should be proportional to each

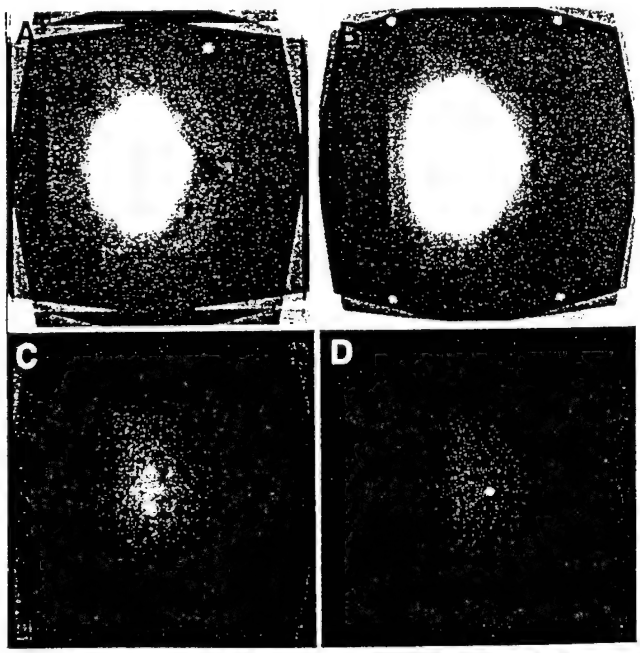

FIGURE 4. Four of 40 ETACT reconstructed slices for case 10/10 (tumor diameter of 10 mm and 10:1 TNT) using 3-mm pinhole. (A) Fifth fiducial plane. (B) Four fiducials. (C) Random slice within breast. (D) Slice containing tumor.

other. Thus, the CNR should be indicative of lesion detectability just as SNR is.

Planar images were simulated for the 10/10 case (which refers to a 10-mm tumor and a TNT of 10:1) and varying pinhole size for comparison with the ETACT reconstructions. The straight lateral view of the breast was simulated with 7 times the counts in a single, simulated ETACT projection. In this way, the planar image had the same total counts as the total ETACT reconstruction. The contrast and the CNR for the planar case were compared with those of the ETACT reconstructed data.

Phantom Experiments

An 8 mm "tumor" was filled with ^{99m}Tc and inserted into the breast phantom (Data Spectrum Corp., Hillsborough, NC). The rest of the breast was filled with water and mixed with ^{99m}Tc to create a 10:1 TNT, 37 kBq/mL (1 mCi/mL) in the breast and 370 kBq/mL (10 mCi/mL) in the tumor. After the phantom was prepared, it was set on a table and 7 projections were taken with a portable gamma camera (TransCam: ADAC Laboratories, Milpitas, CA) using a pinhole collimator. The positioning of the 7 projections was taken to resemble those in the simulation study. Figure 5 displays the experimental setup. The TransCam camera has a 260-mm field of view and a 6.5-mm NaI crystal thickness. This camera has an intrinsic spatial resolution of 3.6 mm and an energy resolution of 10.9% at 140 keV. The data were acquired with a 15% energy window. A 4-mm pinhole was used. Each projection was acquired for 5 min. The total count for each projection was around 45,000. The TACT software was used to reconstruct the data as described. The contrast and CNR measurements were calculated in the same fashion as in the simulation study.

RESULTS

Simulation Results

The simulation results are presented in Tables 2 and 3 and in Figure 6. The labeling 10/5 refers to a tumor size of 10 mm and a TNT of 5:1, whereas 5/10 refers to a tumor size of 5 mm and a TNT of 10:1. Values for all 6 different pinhole sizes are listed. The contrast results are displayed in Table 2. The CNR results are shown in Table 3 and in Figure 6. Our results indicate that a CNR of around 2 is the threshold for detectability. In each case, there is an optimal peak in the CNR curve. The overall optimum is a 3-mm pinhole for a tumor of size 10 mm and a TNT of 10:1. The highest concentration of the best CNRs is as a result of the 3-mm pinhole. Figure 4 shows 4 reconstructed simulations for the 10/10 case. Table 4 compares the contrast and CNR of the planar and ETACT simulations as a function of pinhole size. In all cases, the contrast and CNR for the planar case were less than those for the ETACT case, primarily because of the increased contrast that resulted from the ETACT reconstruction.

TABLE 2
Contrast Measurements

Pinhole size (mm)	Contrast					
	10/10	7.5/10	5/10	10/5	7.5/5	5/5
1	0.472	0.283	0.123	0.254	0.16	0.055
2	0.454	0.262	0.1	0.226	0.145	0.066
3	0.437	0.231	0.068	0.199	0.094	0.049
4	0.375	0.176	0.059	0.149	0.088	0.057
5	0.256	0.148	0.05	0.145	0.078	0.066
6	0.206	0.099	0.055	0.097	0.063	0.058

Case 10/10 refers to 10-mm tumor size and TNT of 10:1, whereas case 7.5/5 refers to 7.5-mm tumor size and TNT of 5:1.

Phantom Results

The results of the phantom experiment including the 8-mm tumor are given in Table 5. Reconstructed slices through the breast, including the fifth marker, the 4 coplanar markers, the breast, and the tumor, are shown in Figure 7. The 8-mm tumor is detectable and these results are comparable with our simulation results.

DISCUSSION

In the simulation experiments, ETACT was shown to have the potential of detecting tumors <1 cm. However, a

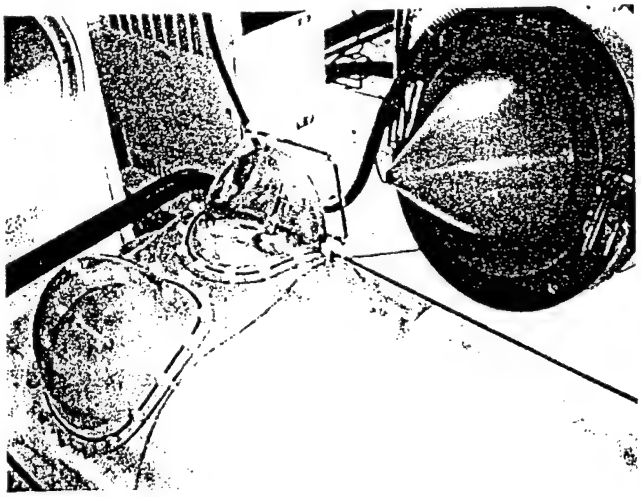

FIGURE 5. Phantom experiment setup includes anthropomorphic phantom and portable gamma camera with pinhole collimator aimed at lateral side of breast. Seven projections were taken of breast at different angles. These projections were then reconstructed using ETACT software to create slices through breast.

TABLE 3
CNR Measurements

Pinhole size (mm)	CNR					
	10/10	7.5/10	5/10	10/5	7.5/5	5/5
1	4.63	2.77	1.21	2.5	1.57	0.54
2	6.98	4.03	**1.54**	3.48	**2.23**	1.02
3	**8.57**	**4.53**	1.33	**3.9**	1.84	0.96
4	7.98	3.74	1.26	3.17	1.87	1.22
5	6.24	3.61	1.22	3.53	1.9	1.61
6	5.72	2.75	1.53	2.7	1.75	**1.61**

Optimum for each case is in boldface type.

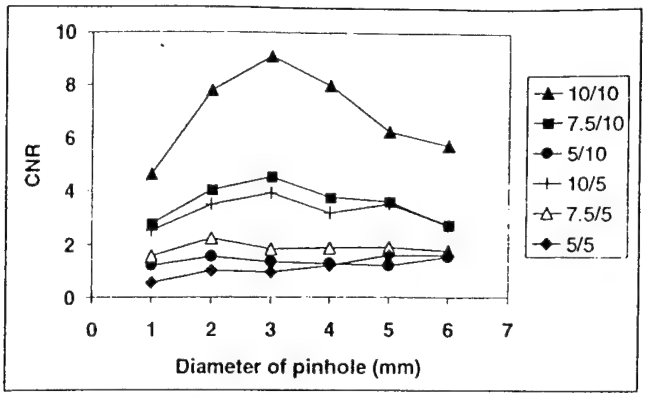

FIGURE 6. Plot of CNR measurements for different simulated cases: as TNT increases, CNR also increases. In most cases, optimal pinhole size is 3 mm.

5-mm tumor was not detectable even for a TNT as high as 15:1. The CNR threshold for detection was determined objectively to be around 2.0. As the pinhole size of the collimator increased, the contrast of the image worsened and the noise decreased; conversely, as the pinhole size decreased, the contrast improved and the noise worsened. Thus, there may be an optimal pinhole size as determined by that that yields the maximal CNR. The optimal pinhole size was observed to be the 3-mm pinhole for all discernable cases, although it was not substantially better than 4 mm. The contrast and CNR were consistently higher for the ETACT simulation compared with a planar simulation.

The simulation study may be limited because attenuation and Compton scatter were not included in the model. Attenuation may have an effect on the final image. γ-Rays from the tumor had to travel half of the breast, but γ-rays from behind the tumor had more tissue through which to travel and thus would be attenuated more. Attenuation may have reduced the image contrast, but the effect would probably be small. In Compton scatter, the photon changes direction as it scatters, causing a loss in spatial resolution and the contrast for small objects to worsen. In the clinic, the limited energy resolution of the NaI crystal in the gamma camera makes it impossible to eliminate all of the Compton scattering. Even with a 15% energy window, scattered radiation will still be incorporated into the image. Therefore, the phantom study results may not exactly match

TABLE 4
Comparison of Simulated Planar and ETACT Data

Pinhole size (mm)	Contrast		CNR	
	Planar	ETACT	Planar	ETACT
1	0.402	0.472	3.98	4.63
2	0.345	0.454	5.43	6.98
3	0.300	0.437	5.58	8.57
4	0.255	0.375	5.13	7.98
5	0.214	0.256	4.40	6.24
6	0.165	0.206	3.25	5.72

TABLE 5
ETACT Phantom Results

Tumor size (mm)	Phantom measurements		
	Contrast	% SD	SNR
8	0.58	15.8	3.67

Measurements were made with 4-mm pinhole.

the simulated data because of attenuation and Compton scatter. On the other hand, it is unclear whether the inclusion of attenuation and Compton scatter has much effect on the comparison of ETACT with other conventional imaging methods because these considerations would affect these methods as well. We are investigating the role of attenuation and Compton scatter in ETACT through Monte Carlo simulations and a comprehensive phantom study.

In the phantom studies, the aim was to create a simulated clinical setting. The breast was filled with a 37-kBq/mL (1 mCi/mL) solution and the tumor was filled with 370 kBq/mL (10 mCi/mL). The phantom was imaged with seven 5-min exposures, a total of 35-min acquisition time, which would be considered a reasonable study time in the clinic. The phantom results are a reasonable indication of what may be expected with real patient data. The phantom results also verified the validity of the simulation results.

To improve the potential of the ETACT method, some aspects of the experimental setup need further investigation:

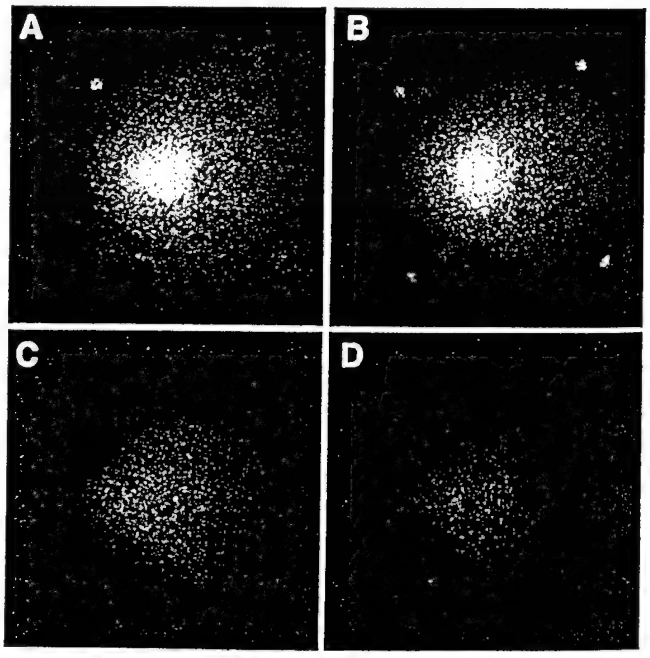

FIGURE 7. Four of 40 reconstructed slices of anthropomorphic phantom using 8-mm tumor size with 10:1 TNT. (A) Fifth fiducial slice. (B) Four fiducials. (C) Random slice within breast. (D) Slice containing 8-mm tumor. As viewed, 8 mm is detectable.

pinhole size, collimator, field of view, angular disparity of the projections, and iterative deconvolution. On the basis of our simulation results, a 3-mm pinhole will be constructed and used for future phantom studies. Simulation results imply that a 6-mm tumor might be visible with the 3-mm pinhole. Another way of improving the resolution, and therefore the SNR, of the images is to increase the field of view of the detector, allowing for more magnification. This could possibly be accomplished by the use of optical markers. Instead of radioactive fiducial markers, visible ones could be used with an optical system mounted to the gamma camera. The optical markers would be used for the reconstruction process. Thus, the gamma camera could more closely approach the patient with more flexibility, but without all of the fiducial markers necessarily being in the field of view of the gamma camera. This could lead to an increase in both resolution and sensitivity. Iterative deconvolution could also improve the results of the ETACT method, by subtracting the unwanted signals from neighboring slices. To fully analyze the ETACT method, a clinical evaluation needs to be performed eventually.

CONCLUSION

We evaluated the scintimammography technique, ETACT, through simulation and phantom experiments. The simulation experiments revealed that the 3-mm pinhole size is the optimum for the best tradeoff between resolution and noise. The phantom studies were consistent with the simulation results and proved that we can get reasonable results in a simulated clinical setting. In the phantom experiments, the 8-mm tumor was visible using the 4-mm pinhole. Therefore, ETACT has the potential to improve patient diagnoses by detecting tumors at an earlier stage and could be applied in any hospital in an easy and flexible manner.

ACKNOWLEDGMENTS

The authors thank Cathy Eades and Zhiping Mu for their help in the performance of these studies. The U.S. Army Medical Research and Materiel Command under DAMD grant 17-98-8349 supported this work.

REFERENCES

1. Overmoyer B. Breast cancer screening. *Med Clin North Am.* 1999;83:1443–1466.
2. Hannon D. Breast imaging: fighting a good fight. *Med Imaging.* 1999;14:38–43.
3. Fraumeni JF Jr, Hoover RN, Devesa SS, Kinlen LJ. Epidemiology of cancer. In: DeVita VT, Hellman S, Rosenberg SA, eds. *Cancer: Principles and Practice of Oncology.* 4th ed. Philadelphia, PA: JB Lippincott; 1993:150–181.
4. Neumann P, Romann D, Camara O, Riedel HH. Possibilities and limits of mammography with special reference to breast carcinoma: a comparison of clinical, mammography and histologic diagnoses [in German]. *Zentralbl Gynakol.* 1997;119:154–159.
5. Khalkhali I, Cutrone J, Mena I, et al. Technetium-99m-sestamibi scintimammography of breast lesions: clinical and pathological follow-up. *J Nucl Med.* 1995; 36:1784–1789.
6. Palmedo H, Schomburg A, Grünwald F, Mallmann P, Boldt I, Biersack HJ. Scintimammography with Tc-99m MIBI in patients with suspicion of primary breast cancer. *Nucl Med Biol.* 1996;23:681–684.
7. Webber RL, Horton RA, Tyndall DA, Ludlow JB. Tuned-aperture computed tomography (TACTTM): theory and application for three-dimensional dentoalveolar imaging. *Dentomaxillofac Radiol.* 1997;26:53–62.
8. Grant G. Tomosynthesis: a three-dimensional radiographic imaging technique. *IEEE Trans Biomed Eng.* 1972;1:20–28.
9. Webber RL, Underhill HR, Freimanis RI. A controlled evaluation of tuned-aperture computed tomography applied to digital spot mammography. *J Digit Imaging.* 2000;13:90–97.
10. Hemler PF, Webber RL, Fahey FH. Modeling and error identification of three dimensional tomosynthetic reconstructions. *SPIE Proc.* 2000;1287:1280–1287.
11. Sorenson JA, Phelps ME. *Physics in Nuclear Medicine.* 2nd ed. New York, NY: Grune & Stratton; 1987:342.

Biorthogonal merging of mammographic slices using Tuned-Aperture Computed Tomography®

Richard L. Webber
Departments of Dentistry and Medical Engineering, Division of Radiologic Sciences
Wake Forest University School of Medicine
Winston-Salem, NC 27157-1093
rwebber@wfubmc.edu

Frederic H. Fahey
Department of Medical Engineering
Wake Forest University School of Medicine
Winston-Salem NC 27157-

This investigation demonstrates a method for creating three-dimensional (3D) mammograms. It involves biorthogonal merging of independent tomographic representations. A test specimen containing human breast tissue with reference points attached was irradiated from five angles and from two orthogonal orientations. Data from both orientations were processed independently to yield data derived from the same tissues but oriented orthogonally. By combining suitably-corrected 3D matrix representations of these data, it was possible to assign more accurate estimates of volume elements in the resulting 3D reconstructions. Data obtained using a conventional digital stereotactic mammography system yielded a merged 3D image that retained spatial details and apparent structural continuity even when rendered as a cube rotated through a full 360•. We conclude that merging 3D matrices derived from multiple projections obtained biorthogonally may offer an intriguing alternative to conventional 2D digital mammography and intrinsically anisotropic 3D mammographic imaging methods.

KEY WORDS: digital imaging, three dimensions, mammography, computed tomography, nonlinear processing

ABSTRACT

This investigation explores the potential for creating three-dimensional (3D) mammograms through biorthogonal merging of independent tomographic representations. A cuboidally shaped test specimen containing human breast tissue with reference points attached to each corner was irradiated from five angles and from two orthogonal orientations, yielding a total of 10 projections. Data from both orientations were processed independently to yield independent laminographic series derived from the same tissues but oriented orthogonally. Relationships derived from respective projections of the reference points were used to correct for cone-beam artifacts. A matrix-rotation program was developed and applied to the data underlying one of these now affine-corrected 3D representations that, in effect, flipped it 90•. By combining the rotated 3D volume representation with its unrotated, orthogonally generated counterpart, it was possible to assign more accurate estimates of volume elements in the resulting 3D reconstructions. Data obtained using a conventional digital stereotactic mammography system yielded a merged 3D image that retained spatial details and apparent structural continuity even when rendered as a cube rotated through a full 360•. We conclude that merging 3D matrices derived from multiple projections obtained biorthogonally may offer an intriguing alternative to conventional 2D digital mammography and intrinsically anisotropic 3D mammographic imaging methods.

1 Introduction

Conventional mammography is an intrinsically two-dimensional (2D) imaging process. As such, its diagnostic potential is necessarily limited by the extent to which essential 3D information is obscured by irrelevant tissue details located either above or below the region of interest. The similarity in attenuation between normal and cancerous breast tissues affects both sensitivity and specificity and is particularly important when the region of interest is small and the enveloping tissue relatively dense. The addition of depth information via conventional stereometry has been shown to improve diagnostic

performance.[1] However, this approach does not allow for suppression of 3D details known to be irrelevant (structured noise).[2]

Conventional computed tomography (CT) provides a theoretically tractable means for isolating questionable tissue patterns in 3D, but anatomical and radiographic restrictions unique to mammographic applications present a formidable challenge to existing CT scanner designs.[3,4] Recent findings by Niklason *et al.*[5] suggest that digital tomosynthesis may provide significant benefits for breast cancer screening. This conclusion was reinforced by the results of a controlled in vitro study demonstrating significantly improved sensitivity for detection of standardized mammography details buried in normal breast tissues when displayed in 3D.[6] However, off-axis projection constraints required by tomosynthetic imaging geometry necessarily induce spatial correlations between reconstructed slices, thereby restricting 3D information to regions outside the associated null space.

2 Experimental Goal

This investigation explores a method for effectively eliminating this shortcoming through the merging of data produced by using multiple orthogonal sampling strategies. More specifically, we test the hypothesis that it is possible to combine data obtained from two (or more) tomosynthetic projection series oriented at right angles to each other to yield a single composite 3D representation that minimizes the sampling gaps associated with the intrinsic "one-sided" reconstruction techniques underlying conventional tomosynthesis.

3 Theoretical Considerations

Before we can achieve this objective, we must solve some technical problems. One such problem is caused by the cone-beam projection geometry used to produce the underlying source projections. All projections produced from a finite focal-object distance necessarily exhibit significant differences in projective magnification from one slice to the next. For this reason, details in planes relatively nearer the x-ray source are magnified more than comparable details located nearer the projection plane. Consequently, a volume that in reality has the shape of a cube appears as a truncated pyramid when rendered tomosynthetically in 3D (Fig.1).

This intrinsic scaling distortion poses no significant problems so long as each slice is interpreted independently. However, when slices produced from conventional projection sequences are to be registered with others synthesized from orthogonally oriented samples, even relatively small variations in projection scaling with depth can preclude accurate spatial registration. We chose to avoid this difficulty by isotropically rescaling each reconstructed slice by an amount calculated to produce unity magnification throughout the volume. Because the results are identical to those that would have been produced using affine projection geometry, we coined the term "affinization" to describe this correction procedure.[7]

Another problem that must be solved is the need for precise registration of homologous volume elements. We dealt with this problem by attaching easily recognized fiducial points to the object of interest. Because these points were positioned in fixed known locations, the affinization process described

above was easy to perform. Moreover, the reconstruction process was rendered more precise by eliminating any projection inaccuracies associated with rigid coupling of the object to the projection system. This simplification arises from the use of these same fiducial points to accomplish the 3D reconstruction using Tuned-Aperture Computed Tomography® in lieu of conventional tomosynthesis.[8,9] Finally, precise registration of the two resulting affinized 3D volumes was accomplished through the straightforward process of projective superposition.

4 Materials and Methods

This approach was used to image some frozen human breast tissue known to contain calcified blood vessels and characteristic microcalcifications. Multiple slices of this tissue ranging in thickness from 10 to 12 mm were stacked and cut into squares that would fit snugly into a 35 mm cardboard film box measuring 38 x 38 x 53 mm. Lead spheres approximately 2 mm in diameter (Y-Spots, Beekley Corp., Bristol, CT USA) were attached to the four bottom corners of the box, and four more were attached to the vertical edges at a distance 38 mm up from the base. This procedure yielded a cube-shaped region containing frozen breast tissue bounded at each vertex by easily recognized radiopaque markers (Fig. 2).

This container was radiographed as shown in Fig. 2 from five discrete angles using a modified mammography machine configured with a swing arm and a digital camera attachment used in stereotactic applications (Delta 16, Instrumentarium Imaging, Tuusula, Finland). Note that the position of the box was shifted laterally slightly between successive exposures to assure that all eight fiducial reference points were always projected onto the region defined by the digital detector when the position of the x-ray source changed. The resulting mammographic projections had angular disparities of approximately -15°, -7.5°, 0°, 7.5°, and 15° from vertical. Five anteroposterior (AP) images were obtained under these conditions using default settings for kVp and exposure as determined by the automatic exposure system on the machine. The box then was rotated 90° about an axis perpendicular to the front and rear faces of the cube, and the lateral projection series (LAT) was repeated using the same settings. This procedure yielded the two orthogonal projection sets shown in Fig. 3.

These two orthogonal sets were used to produce two independent series of 165 tomosynthetic slices each. To minimize the introduction of known tomosynthetic artifacts into the reconstruction of individual slices caused by unregistered projections of high-contrast structures located outside the plane of

interest, we used two different deblurring techniques, one linear and one nonlinear. The linear method involved the application of an iterative deconvolution scheme based on the known point-spread function underlying the 3D reconstruction process.[10] The nonlinear method involved minimization of respective pixel values as opposed to the averaging process underlying conventional back-projection algorithms.[11] It has been suggested that this expedient may increase observer specificity for radiopaque signals at the expense of sensitivity.[12] As described above, these slices were then affinized individually by proportional re-projection of each, relative to fixed positions established by the shadows produced from the four coplanar fiducial points located closest to the plane of the digital detector. Slight inaccuracies caused by the imperfect placement of the fiducial points on the exact corners of a cube, likewise, were corrected in this way, thus assuring that each slice within the confines of the cube was remapped into a perfect square. Cropping each resultant 3D matrix (stack of slices) to only the volume enclosed by the cube produced two independent representations of the same volume from the two original orthogonal projection sets. Shifting corresponding voxel addresses from one matrix such that they reference homologous volume elements in the other permitted merging of these independent data sets through simple averaging of corresponding slices. The resulting 3D matrices were then rendered using either linear averaging or nonlinear maximum-brightness ray-tracing schemes. The results were a series of conventional-appearing 2D projections that could be selected interactively or displayed in rapid sequence through a series of contiguous angles spanning a full 360°.

5 Results

Fig. 4 shows a series of representative projections produced using a maximum-brightness rendering scheme generated from the merged 3D data and from both unmerged 3D components. For these examples the underlying slice reconstructions were the result of linearly deconvoluted back projections. They are arranged in such a way that each row shows the effect of a 90° rotation through an increment of 45°. The middle row illustrates the effect of merging the 3D matrices seen in the top and bottom rows produced from the AP and LAT orthogonal data sets, respectively. Notice that the interslice correlations produced from the limited angular disparity associated with tomosynthetic sampling geometries create large streak artifacts. These are particularly evident when the 3D reconstructions are viewed at angles significantly greater (45° and 90°) than the maximum disparity of the source projections (30°) underlying

each of the separate orthogonally sampled matrices. The superiority of the projections produced from the merged data (middle row) is obvious, especially when compared with Figs. 4(b) and 4(c) (top row) and 4(g) and 4(h) (bottom row). Notice also the significant artifactual streaking of the high-contrast structures caused by the linear back-projection reconstruction method even in 4(a) and 4(i), the unrotated, optimally projected images.

These artifacts appear much less obvious in the comparable projections shown in Fig. 5. The only difference between these renderings and those seen respectively in Fig. 4 is the use of the nonlinear minimization algorithm described above instead of iteratively deconvoluted linear back projections for the underlying 3D image reconstructions. Although these images contain fewer obscuring streak artifacts than those seen in Fig. 4, by virtue of their intrinsic nonlinearity they necessarily introduce significant errors of omission that may, or may not, interfere with image interpretation depending on the diagnostic task involved. Indeed, the nonlinear methods used to accomplish the merging process as demonstrated above necessarily reject most of the information produced from the 10 basis projections.

The results displayed in Fig. 6 illustrate the opposite effect. Here, the reconstructions and renderings were accomplished using all linear methodology. This is to say that the merged reconstructions were derived from iteratively deconvoluted back projections, and the resulting projections were rendered using averaging in lieu of the maximum brightness algorithm underlying the displays shown in Fig. 4. Notice the relative retention of fixed-pattern artifacts intrinsic to redundant projective sampling geometry in Fig. 6. For example, these blurring artifacts tend to obscure the calcified blood vessel and other diagnostic details in projections rotated significantly from the projection geometry underlying the original source projections.

6 Discussion

Irrespective of the choice of algorithms selected for 3D reconstruction and display, these results appear to be consistent with our hypothesis that artifacts produced by anisotropic sampling intrinsic to tomosynthetic projection geometries can be mitigated through redundant sampling made possible by integration of multiple data sets. Limiting redundant samples to mutually orthogonal projection geometries as demonstrated in this investigation also assures that the number of required projections for anisotropic sampling can be minimized. However, there is no theoretical restriction of this approach for minimizing

null spaces that limits the merging of 3D data to those produced solely from orthogonal projection geometries. Indeed, any sampling scheme that permits independent estimates of a common 3D volume to be realized can be conceivably integrated into a more uniform and, hence, less distorted 3D representation.

In this instance one can opt to use conventional linear reconstruction and rendering methods that theoretically retain most of the information contained in the source projections but often obscure desired details with the intrinsic tomographic blur associated with correlated image sampling within a given projection series. Alternatively, one can employ one or more nonlinear processing options that necessarily reduce the relative amount of information retained with the intent that their use also excludes undesired information such as correlated blur produced from out-of-focus structures. As demonstrated in Figs. 4, 5, and 6, either option can yield improved 3D image quality at extreme angles through the expedient of biorthogonal merging of independently sampled sets of projection data.

The residual streaking of high-contrast structures from the merged data (middle rows of Figs. 4, 5, and 6) is likely aggravated by the fact that the total angular disparity (30°) used to produce each component projection set does not encompass the entire range of projection angles (see Fig. 7). We are currently testing this hypothesis in another radiographic application by using a more uniform sampling strategy involving biorthogonal merging, wherein the use of angular disparities approaching the required 90° is more easily accomplished.

We also recognize that the simple merging technique demonstrated here most likely is not optimized for many, if not most, common mammographic applications. We suspect, for example, that sophisticated strategies based on maximum likelihood criteria might be more appropriate for certain specific detection tasks. Again, we plan to explore such task-specific options more rigorously in the future.

7 CONCLUSIONS

We have demonstrated that it is possible to combine 3D information, derived from two independent orthogonally oriented sets of x-ray projections, into a single unified 3D image that can be visualized from any angle with fewer of the intrinsic correlation artifacts associated with conventional tomosynthetic reconstruction schemes. Moreover, the use of nonlinear methods for reconstruction and display of the resulting merged 3D information can produce sharp-appearing renderings from a broad range of angles that appear to be all but clinically uninterpretable when rendered by conventional back-projection

algorithms. However, rational interpretation of the relatively blur-free nonlinearly processed images as demonstrated here is appropriate only for specific diagnostic tasks that can be shown to be uninfluenced by the inevitable information losses associated with these filtering schemes.

Acknowledgment

This work was supported in part by National Institutes of Health Grant No. 5 RO1 CA74106.

References

1. M. May, "Three-dimensional mammography," *Am. Scientist* 82, 421-422 (1994).
2. H. L. Kundel and G. Revesz, "Lesion conspicuity, structured noise, and film reader error," *AJR Am. J. Roentgenol.* 126, 1233-1238 (1976).
3. S. L. Edell and M. D. Eisen, •Current imaging modalities for the diagnosis of breast cancer," *Del. Med. J* . 71, 377-382 (1999).
4. J. W. T. Muller, P. F. G. M. van Waes, P. R. Koehler, "Computed tomography of breast lesions: comparison with x-ray mammography, " *J. Comput. Assist. Tomogr.* 7, 650-654 (1983).
5. L. T. Niklason, B.T. Christian, L. E. Niklason, D. B. Kopans, D. E. Castleberry, B. H. Opsahl-Ong, C. E. Landberg, P. J. Slanetz, A. A. Giardino, R. Moore, D. Albagli, M. C. DeJule, P. F. Fitzgerald, D. F. Fobare, B. W. Giambattista, R. F. Kwansnick, J. Liu, S. J. Lubowski, G. E. Possin, J. F. Richotte, C. Y. Wei, R. F. Wirth, "Digital tomosynthesis in breast imaging," *Radiology* 205, 399-406 (1997).
6. R. L. Webber, H. R. Underhill, R. I. Freimanis, "A controlled evaluation of tuned-aperture computed tomography applied to digital spot mammography," *J. Digit. Imag.* 13, 90-97 (2000).
7. T. M. Persons, P. F. Hemler, R. L. Webber, H. R. Underhill, "Elimination of tomosynthetic artifacts through integration of orthogonal volume sets," *Medical Imaging 1999: Physics of Medical Imaging*, Proc. SPIE 3659, 925-932 (1999).
8. Webber RL, inventor; Wake Forest University, assignee; "Self-calibrated tomosynthetic, radiographic-imaging system, method and device," US patent 5,359,637 (1994 Oct 25).
9. Webber RL, inventor; Wake Forest University, assignee; "Self-calibrated tomosynthetic, radiographic-imaging system, method and device," US patent 5,668,844 (1997 Sept 16).

10. U. E. Ruttimann, R. A. J. Groenhuis, R. L. Webber, "Restoration of digital multiplane tomosynthesis by a constrained iteration method," *IEEE Transactions on Medical Imaging*, MI-3, 141-148 (1984).

11. R. L. Webber, P. F. Hemler, J. Lavery, "Objective evaluation of linear and nonlinear tomosynthetic reconstruction algorithms," *Medical Imaging 2000: Technology Evaluation and Observer Performance*, Proc. SPIE 3981, 224-231 (2000).

12. R. L. Webber, H. R. Underhill, P. F. Hemler, J. Lavery, "A nonlinear algorithm for task-specific tomosynthetic image reconstruction," *Medical Imaging 1999: Physics of Medical Imaging,* Proc. SPIE 3659, 258-265 (1999).

FIGURE CAPTIONS

Fig. 1 Diagram showing distortion of 3D shape produced by cone-beam projection geometry.

Fig. 2 Diagram showing projection geometry and detail of the breast specimen encased in a cube-shaped container with fiducial markers.

Fig. 3 Two independent series of five x-ray projections of the breast specimen, one oriented predominantly anteroposteriorly showing a calcified blood vessel (left column), and the other oriented predominantly laterally showing multiple adjacent layers of breast tissue (right column).

Fig. 4 Three series of linearly reconstructed (back-projected) images rendered with a nonlinear (maximum-brightness) ray-tracing scheme shown at various angles comparing images produced with and without biorthogonal merging.

Fig. 5 Three series of nonlinearly reconstructed (minimized) images rendered with a nonlinear (maximum-brightness) ray-tracing scheme shown at various angles comparing images produced with and without biorthogonal merging.

Fig. 6 Three series of linearly reconstructed (back-projected) images rendered with a linear (average) ray-tracing scheme shown at various angles comparing images produced with and without biorthogonal merging.

Fig. 7 Diagram showing undersampled regions produced by the 30° angle associated with the projection geometries underlying all of the 3D reconstructions in this report.

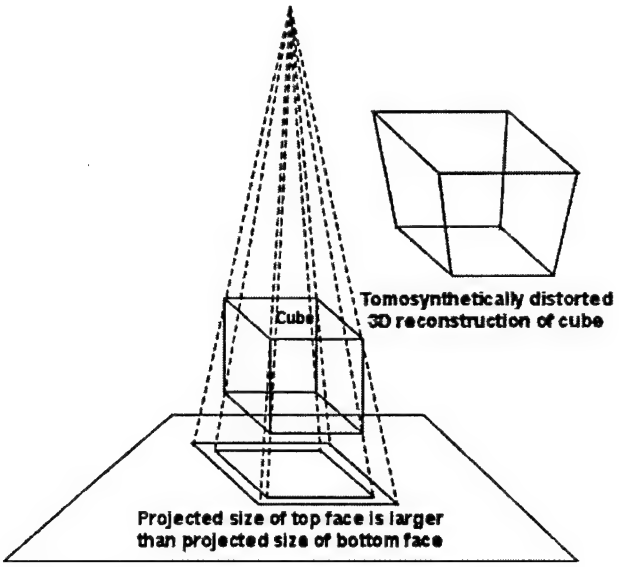
Tomosynthetically distorted
3D reconstruction of cube
Cube
Projected size of top face is larger
than projected size of bottom face

Fig. 1

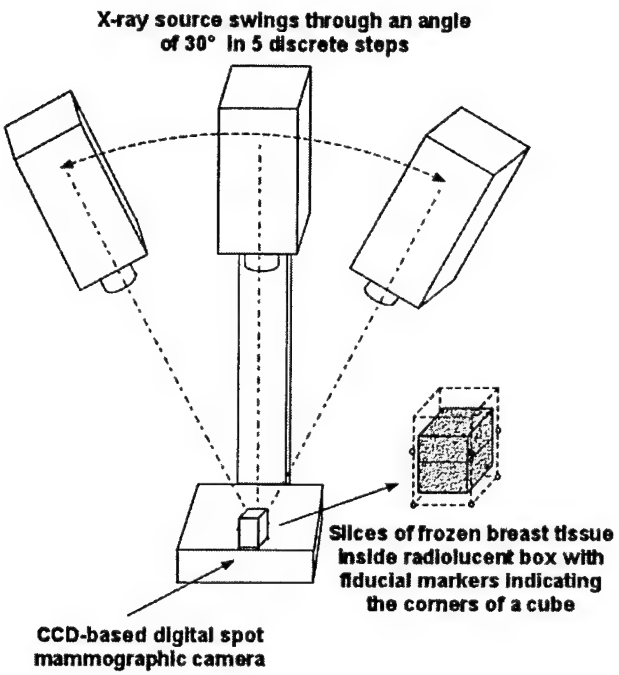
X-ray source swings through an angle
of 30° in 5 discrete steps
Slices of frozen breast tissue
inside radiolucent box with
fiducial markers indicating
the corners of a cube
CCD-based digital spot
mammographic camera

Fig. 2

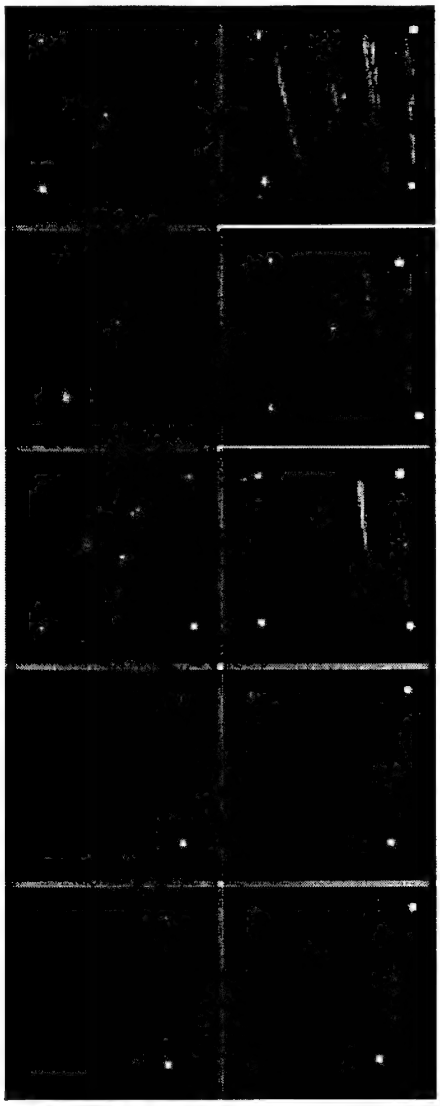

Fig. 3

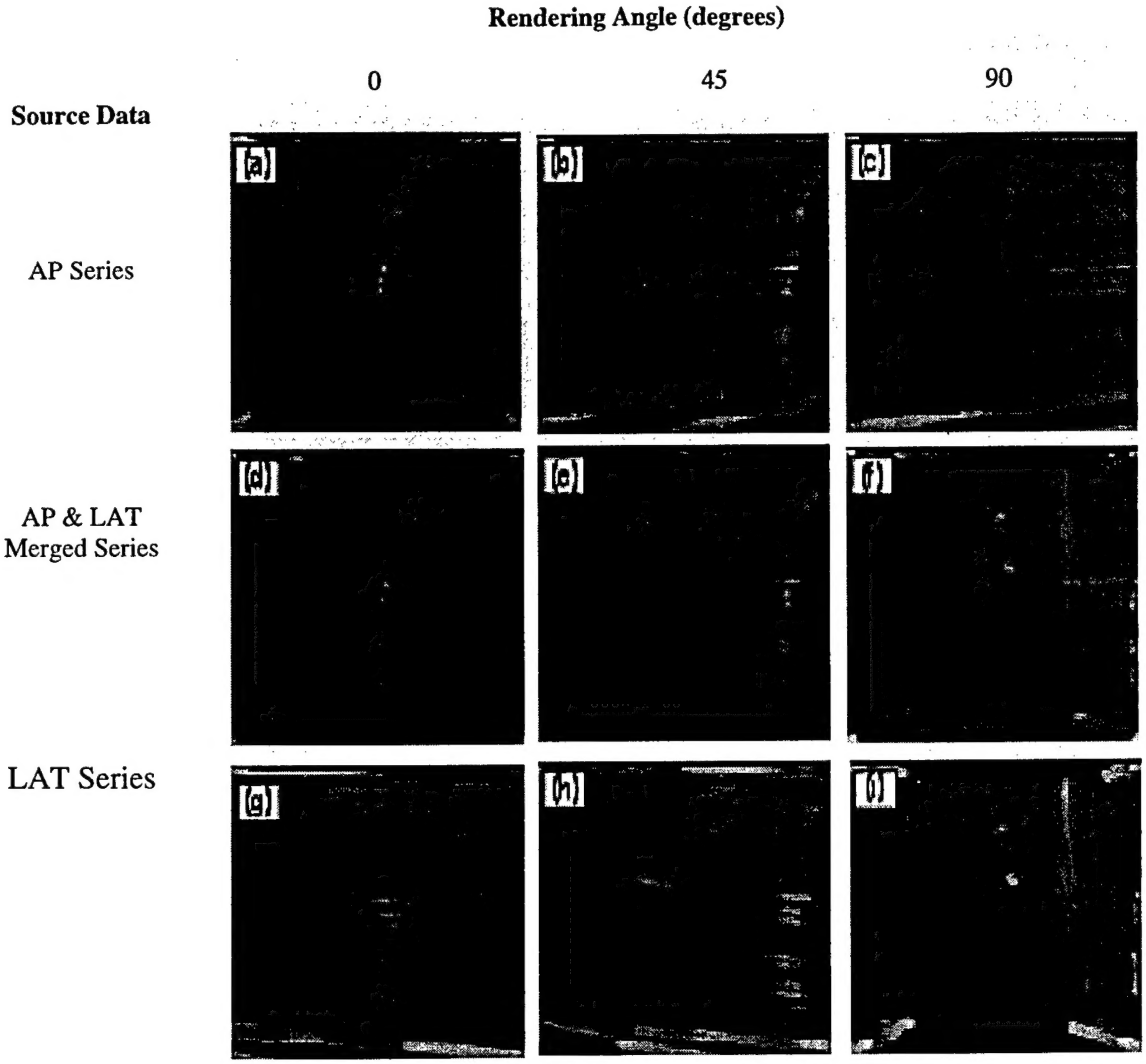
Rendering Angle (degrees)
0
45
90
Source Data
AP Series
AP & LAT
Merged Series
LAT Series
(a)
(b)
(c)
(d)
(e)
(f)
(g)
(h)
(i)

Fig. 4

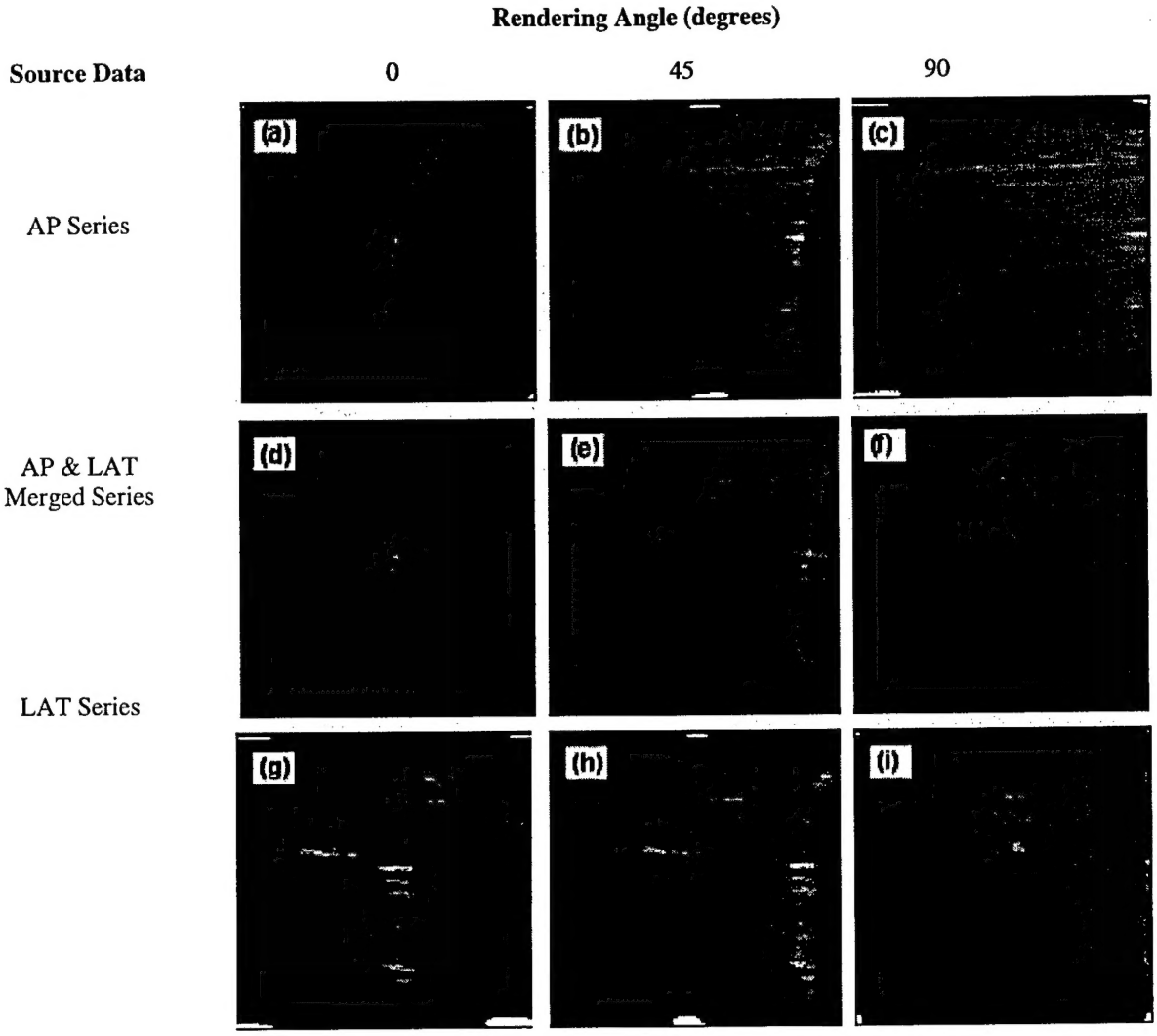
Rendering Angle (degrees)
Source Data
0
45
90
AP Series
AP & LAT Merged Series
LAT Series
(a)
(b)
(c)
(d)
(e)
(f)
(g)
(h)
(i)

Fig. 5

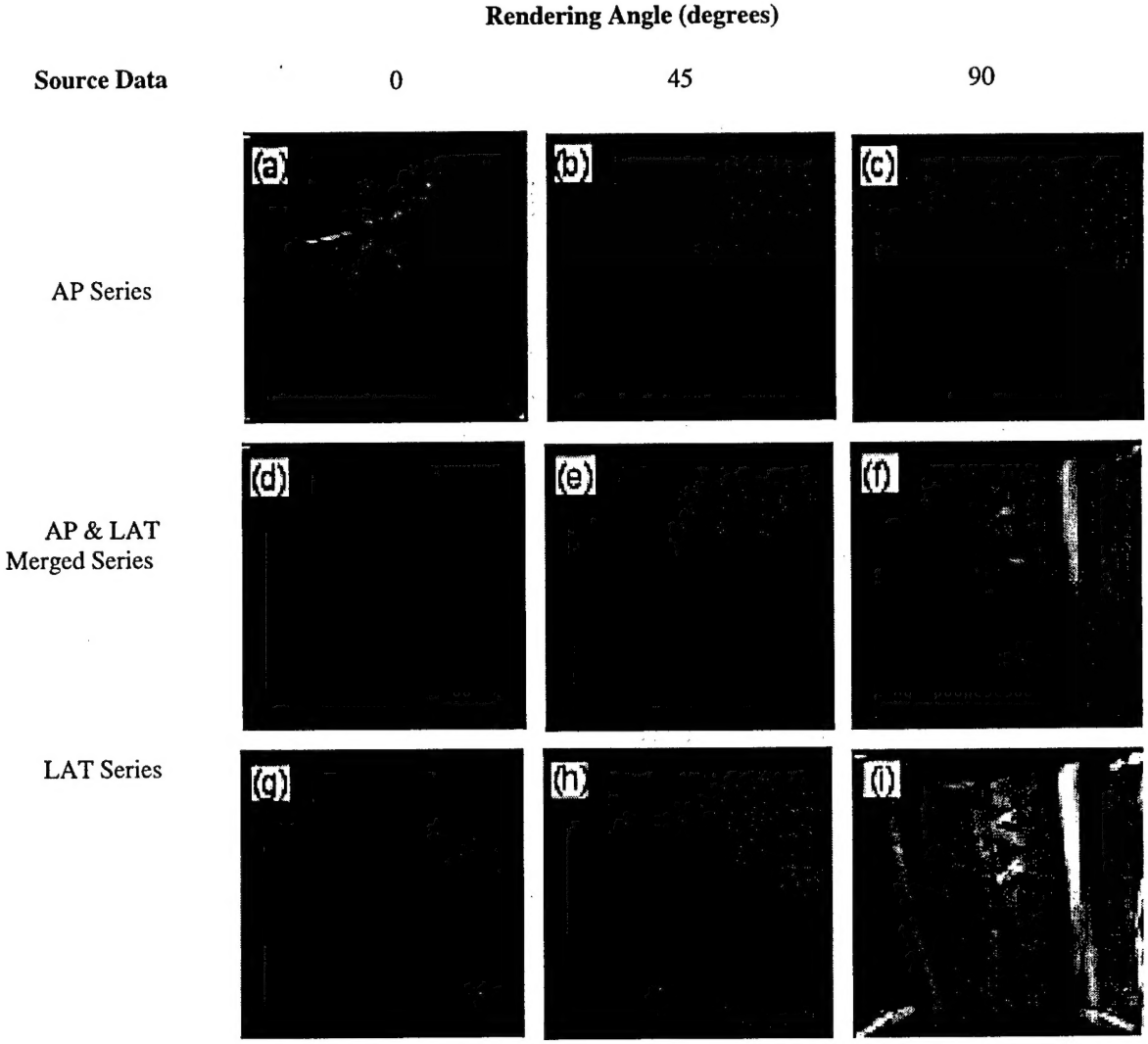
Rendering Angle (degrees)
Source Data
0
45
90
AP Series
AP & LAT Merged Series
LAT Series
(a)
(b)
(c)
(d)
(e)
(f)
(g)
(h)
(i)

Fig. 6

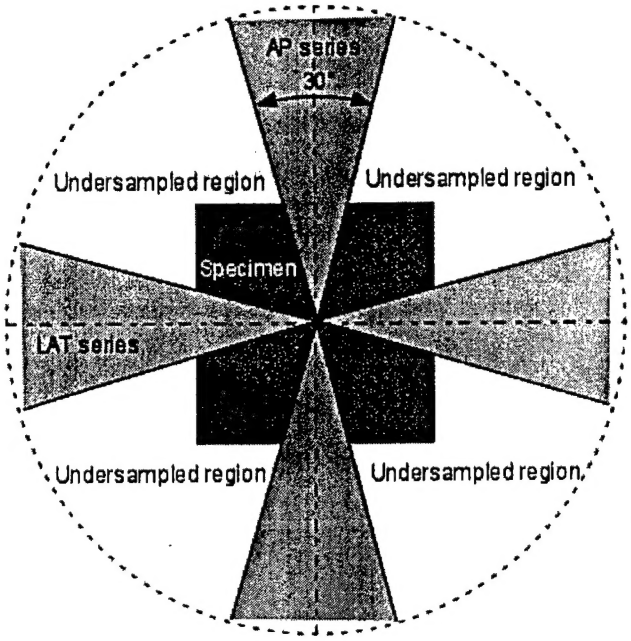
AP series
30°
Undersampled region
Undersampled region
Specimen
LAT series
Undersampled region
Undersampled region
Axial View

Fig. 7